ACS OMEGA

Open Access



http://pubs.acs.org/journal/acsodf

Article

# Role of the Metal Precursor in Preparing Dual-Atom Catalysts for the Oxygen Reduction Reaction

Xiu Zhu, Genlin Liu, Xiafang Tao, Pengwei Huang, Qing Wang, Guangbo Chen,* Juan Yang, Liang Zhang, and Yazhou Zhou*

Cite This: *ACS Omega* 2023, 8, 41708−41717

Read Online

ACCESS | Metrics & More | Article Recommendations | Supporting Information

**ABSTRACT:** Dual-atom catalysts (DACs) have arisen as a novel type of heterogeneous catalyst that extends from single-atom catalysts (SACs) by incorporating two kinds of metals. These materials have demonstrated enhanced performance when compared to SACs. The choice of metal precursors plays an important role in the synthesis of DACs. Here, we choose Fe and Co as DAC models and study types, contents, molar ratios of two precursors, and oxygen reduction reaction (ORR) activity. The Fe,Co DACs were synthesized by an adsorption−annealing approach, using nitrogen-doped graphitic carbon (NC) as the support. As a result, the adsorption ability of metal precursors on the support determines the metal loadings in Fe and Co DACs, leading to differences in ORR performance. The Fe precursors win the adsorption competitions in most cases, resulting in a much higher loading than that of Co precursors. Importantly, it is difficult to increase the precursor content by simply increasing the initial amount. Choosing the right combination of metal precursors, such as ferrocene and cobalt chloride, can yield Fe,Co DACs with enhanced ORR performance..

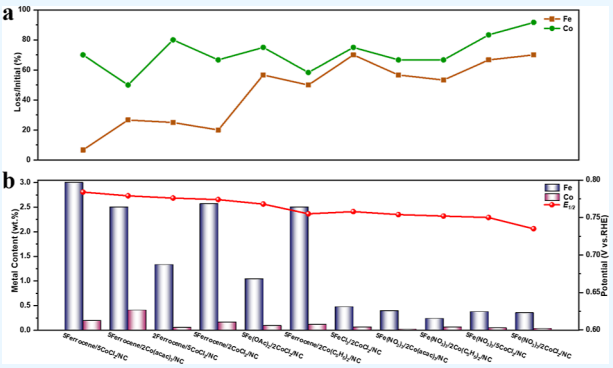


## INTRODUCTION

Single-atom Fe−N−C materials have emerged as promising alternatives to platinum-group metal materials (PGM) in proton exchange membrane fuel cells (PEMFCs) because of a good oxygen reduction reaction (ORR) activity in acidic solution.[1−4] Single-atom Fe coordinated with nitrogen atoms (e.g., $FeN_4$) is considered the main active site.[5−7] However, the strong adsorption ability of the central Fe toward ORR-related intermediates significantly hampers the ORR kinetics.[8−10] Nevertheless, the active Fenton reaction of Fe toward $H_2O_2$ during the ORR process causes severe demetalation and free radicals, leading to poor durability, particularly for PEMFC environments.[11−13]

Various strategies have been proposed to further improve the ORR performance of Fe−N−C materials: (1) regulation of the electronic structure of the central Fe by the incorporation of secondary heteroatoms such as S, P, B, and F into the first coordination shell of Fe or doped into carbon structures;[14−18] (2) increasing the site density of Fe active sites;[6,19,20] and (3) introducing the secondary metals for the formation of dual-atom catalysts (DACs).[21−24] DACs have been defined as two metals atomically dispersing on the supports, where single-site metals are either randomly dispersed on supports without the formation of metal−metal interaction[25−27] or the adjacent metal atoms exhibit metal−metal bonds.[28−30] In particular, Fe−Co DACs are being widely investigated and demonstrated to have excellent ORR activity by optimizing the adsorption energy of the actives toward ORR intermediates. Li and co-workers[31] demonstrated that the excellent activity of Fe−Co DACs is attributed to the reduction of the cleavage barrier of the O−O bond on Fe−Co dual sites. Han et al.,[32] claimed that a combination of Fe and Co can change the charge density of metal sites, thereby optimizing the electronic structure and enhancing the ORR activity. There are many methods to synthesize DACs, such as the host−guest method that encapsulates metal precursors within zeolitic imidazolate frameworks (ZIFs)[31,33−35] and the adsorption−annealing approach.[36−39] Many factors including pyrolysis conditions,[40−42] substrates,[43−45] and the etching process[46,47] have been investigated, but their mechanisms are still elusive. Additionally, the features of the metal precursors, such as their reactivity, thermal stability, and adsorption capacity on supports, can potentially influence DAC performance, which is barely reported.

**Received:** August 14, 2023
**Accepted:** September 14, 2023
**Published:** October 24, 2023

Herein, we chose Fe and Co as DAC models to reveal the significance of the choice of metal precursors for constructing DACs. Fe−Co DACs were prepared via the adsorption−annealing method in which nitrogen-doped graphitic carbon (NC) was used as the support for adsorbing metal precursors. The correlation of metal precursors (i.e., types, contents, and molar ratios of Fe and Co precursors) and acidic ORR activity was obtained. The results demonstrated that the metal loadings and ratios of the two metals in Fe−Co DACs are dependent on the metal precursors. Surprisingly, Fe dominates in most cases. The ORR performance results show that the activity of Fe, Co DACs is influenced by the ratios of Fe and Co. However, increasing the Co loading is very challenging because Fe precursors win the adsorption competition with Co precursors on NC supports in most cases. Our work will help us understand in depth the formation of DACs and provide guidance for more precise synthesis.

## EXPERIMENTAL SECTION

**Chemicals.** Zinc nitrate hexahydrate [$Zn(NO_3)_2{\cdot}6H_2O$], 2-methylimidazole, sodium chloride (NaCl), hydrochloric acid (HCl), graphene oxide (GO), melamine, ferrocene, ferric acetate [$Fe(OAc)_2$], ferric nitrate nonahydrate [$Fe(NO_3)_3{\cdot}9H_2O$], ferric trichloride hexahydrate ($FeCl_3{\cdot}6H_2O$), cobalt chloride hexahydrate ($CoCl_2{\cdot}6H_2O$), cobaltocene [$Co(C_5H_5)_2$], cobalt acetylacetonate [$Co(acac)_3$], methanol, and ethanol were used.

**Preparation of the NC Support.** A 500 mL methanol solution containing 7.88 g of 2-methylimidazole was added slowly to a 100 mL methanol solution containing 6.76 g of $Zn(NO_3)_2{\cdot}6H_2O$. After the reaction proceeded for 24 h, the resulting precipitate was washed with methanol and ethanol 3 times and then dried at 60 °C in a vacuum oven. 1.5 g of ZIF-8 and 1.5 g of NaCl powder were ground for 20 min to obtain the mixed powders. The powders were annealed at 910 °C under an Ar atmosphere for 2 h. The resulting black powders were added into a 20 mL HCl solution (2 M). After stirring at 80 °C for 8 h, the black powders were washed with deionized (DI) water and ethanol 6 times by the centrifuging process, followed by a drying process at 60 °C in a vacuum oven.

**Preparation of Fe, Co DACs.** A 50 mg portion of NC was dispersed in 100 mL of methanol after sonication for 2 h. A 5 mL methanol solution containing a certain amount of the metal precursor was added to the above NC solution with 2 h sonication. After stirring for 12 h, the starting materials were collected after a centrifuged washing process with methanol and a drying process overnight at 60 °C in a vacuum oven. The starting materials were labeled as *n*Fe precursor-*m*Co precursors-NC, where *n* and *m* refer to the molar ratios of the initial Fe and Co precursors, respectively. The resulting starting materials were annealed at 900 °C for 1 h under an Ar atmosphere. The catalysts were denoted as *n*Fe precursor/*m*Co precursor/NC, where *n* and *m* refer to the molar ratios of initial Fe and Co precursors, respectively. The details of all combinations in this work can be seen in Table S1.

**Characterizations.** X-ray diffraction (XRD) patterns were recorded by an X-ray diffractometer (Rigaku SmartLab SE) via a Cu K$\alpha$ source with a step of $\lambda$ = 1.54 Å. Raman spectroscopy (Raman) was performed using a micro-Raman spectrometer (Thermo Fisher) excited by a 532 nm laser. The morphology was analyzed by scanning electron microscopy (SEM, Hitachi Regulus-8100) and transmission electron microscopy (TEM, Hitachi H-7800). High-resolution TEM (HR-TEM) images (FEI Tecnai F20), together with element mapping images, were acquired on a JEOL-2100F and an aberration-corrected high-angle annular dark-field scanning TEM (AC-HAADF-STEM) system (JEOL JEM-ARM 200). The Brunauer−Emmett−Teller (BET) surface areas were carried out by the (Quantachrome Autosorb-IQ-MP, $N_2$) surface area analyzer. Inductively coupled plasma optical emission spectroscopy (ICP-OES) was carried out on an Agilent 5110. X-ray photoelectron spectroscopy (XPS) experiments were conducted on a Thermo Scientific K-Alpha spectrometer with an excitation source of Al K$\alpha$. The contents of Fe and Co in the centrifuged supernatant were detected by an atomic absorption spectrometer (AAS CONTR AA300, in $C_2H_2$ air, the wavelength of Fe is 248 nm and that of Co is 240 nm). Thermogravimetry analysis (TGA) was performed on an STA 449 F3 instrument (Ar fluid, 20 °C/min). X-ray absorption spectroscopy (XAS) was performed at the Shanghai Synchrotron Radiation Facility (SSRF) (beamline 11B) and Beijing Synchrotron Radiation Facility (BSRF) (beamline 1W1B).

**Electrochemical Measurement.** Electrochemical measurements were conducted in a three-electrode cell at room temperature (~25 °C) on a CHI 760E electrochemical workstation. The glassy carbon rotating disk electrode (RDE), the rotating ring disk electrode (RRDE), Hg/$Hg_2SO_4$, and a carbon rod were utilized as the working electrodes, reference electrode, and counter electrode, respectively. The catalytic ink was prepared by dispersing 2 mg of catalysts in a solution containing 8 $\mu$L of Nafion (sigma, 5 wt %) solution and 392 $\mu$L of ethanol after 2 h sonication. 30 $\mu$L of catalytic ink was loaded on a glassy carbon electrode, leading to the loading of about 0.76 mg $cm^{-2}$. ORR performance was tested by cyclic voltammetry (CV) in $N_2$- and $O_2$-saturated 0.5 M $H_2SO_4$ with a scanning rate of 50 mV $s^{-1}$. The ORR polarization curves were recorded in an $O_2$-saturated 0.5 M $H_2SO_4$ solution with a rotation speed of 900 rpm and a scanning rate of 5 mV $s^{-1}$. The ORR durability was investigated by continuous potential cycling in an $O_2$-saturated 0.5 M $H_2SO_4$ solution between 0.6 and 1.0 V vs RHE with a scan rate of 100 mV $s^{-1}$. Four-electron selectivity by the RRDE technique was determined by measuring the ring voltage at 1.3 V and calculating the $H_2O_2$ yield. All testing potentials were standardized to potential versus the reversible hydrogen electrode (RHE) according to the following equation.

$$E(RHE) = E(Hg/Hg_2SO_4) + E_0(Hg/Hg_2SO_4) + 0.059\times pH \quad (1)$$

The yield of hydrogen peroxide and the number of electron transfers are calculated by the following equations

$$H_2O_2\ (\%) = 200 \times \frac{\frac{i_r}{N}}{i_d + \frac{i_r}{N}} \quad (2)$$

$$n = 4 \times \frac{i_d}{i_d + \frac{i_r}{N}} \quad (3)$$

$i_r$ is the ring current, $i_d$ is the disk current, and $N$ = 0.37 is the Pt ring current.

**Quantification of the Active Sites.** The active site density (SD) in the 5Ferrocene/2$CoCl_2$/NC, 5$Fe(OAc)_2$/2$CoCl_2$/NC, 5$Fe(NO_3)_3$/2$CoCl_2$/NC, and 5$FeCl_3$/2$CoCl_2$/NC catalysts was measured using the method described by


https://doi.org/10.1021/acsomega.3c06005
ACS Omega 2023, 8, 41708−41717

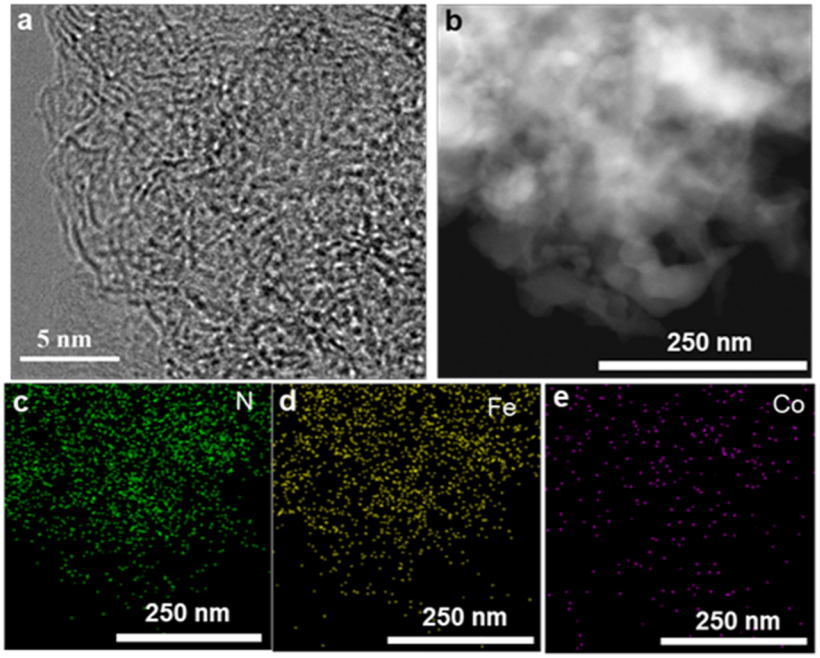


**Figure 1.** (a) HR-TEM image, (b) STEM image, and the elemental mappings of (c) N, (d) Fe, and (e) Co for 5Ferrocene/2$CoCl_2$/NC.

Kucernak[48] et al. The site density was calculated using the following equations[5]

$$SD_{mass}\ (\text{site g}^{-1}) = \frac{Q(\text{AV cm}^{-2})^{*}N_A(\text{atom mol}^{-1})}{n^{*}W(\text{Vs}^{-1})^{*}F(\text{sA mol}^{-1})^{*}L(\text{g cm}^{-2})} \quad (4)$$

where $Q$ is the enlarged area, $N_A$ is the Avogadro constant ($N_A = 6.02 \times 10^{23}$), $F$ is the Faraday constant ($F$ = 96,485 C $mol^{-1}$), $n$ is the number of electrons associated with the reduction of one nitrite per site ($n$ = 5), and $L$ is the catalyst loading during the reversible nitrite poisoning experiments (0.27 mg $cm^{-2}$).

## RESULTS AND DISCUSSION

The Fe, Co DACs were synthesized by an adsorption−annealing approach, using NC as supports and ferrocene, $FeCl_3$, $Fe(OAc)_2$ or $Fe(NO_3)_3$, and $CoCl_2$ as metal precursors. The NC with a high surface area (1775 $m^2\ g^{-1}$) was prepared by the NaCl-assisted pyrolysis of ZIF-8. The SEM and TEM images visualized the identical morphology of all samples to that of NC supports (Figures S1−S3). No metal-based clusters and nanoparticles were observed from the HR-TEM images (Figures 1a and S4), indicating that metals were potentially dispersed atomically on the NC supports. The corresponding elemental mapping images of the representative 5Ferrocene/2$CoCl_2$/NC indicated the coexistence of Fe and Co metals in the sample (Figure 1b−e).

The distributions of metal atoms were observed directly in the AC-HAADF-STEM image. The lower-resolution AC-HAADF-STEM image does not show obvious aggregates (Figure 2a), and some pairs of metal atoms (marked by red circles) with a small site distance of ∼2.5 Å were also evidently observed (Figure 2b), implying the formation of dual-atom sites. The XRD analyses (Figure 2c) show similar diffraction peaks at around 26 and 43°, which are attributed to the (002) and (101) planes of graphitic carbon, respectively. Figure S5 shows the Raman spectra of 5Ferrocene/2$CoCl_2$/NC, 5Ferrocene/NC, and 2$CoCl_2$/NC. The peaks at 1340 and 1580 $cm^{-1}$ belong to the disordered carbon (D band) and graphite carbon (G band),[14,49] respectively. Compared with 5Ferrocene/2$CoCl_2$/NC and 2$CoCl_2$/NC, 5Ferrocene/NC exhibits a higher $I_D/I_G$ of 1.27, indicating the higher density of defects formed in NC supports. The absence of metal-based crystalline particles in the XRD pattern is consistent with the TEM results.

The surface elemental information on the samples was determined by XPS. The XPS survey spectra confirmed the coexistence of N, Fe, and Co in the carbon support. The spectrum was calibrated using the C 1s peak at 284.6 eV. Figure 2d performs almost identical resolution C 1s. The peak at 285.9 eV is assigned to the bonding of C−N, indicating the formation of N-doped carbon.[50,51] Figure 2e shows the N 1s XPS spectra. All samples exhibit similar N contents (Table S2). Through deconvoluting the high-resolution N 1s spectrum, the peaks at 398.4, 399.2, 400.1, 401.1, and 403.1 eV are observed, corresponding to pyridinic-N, M−N (M = Fe or Co), pyrrolic-N, graphitic-N, and oxidized-N species, respectively.[52−56] The types of N and their contents are summarized in Table S3. The results showed that the graphitic N and pyridinic-N are the main N structures. The presence of M−N peaks suggested that the metal atoms are stabilized by nitrogen. Due to the low surface atomic contents in the XPS test, the Fe 2p and Co 2p spectra of all the samples cannot be assigned to the apparent peak (Figure S6).

The fine atomic structure, chemical state, and coordination environments of Fe and Co species in 5Ferrocene/2$CoCl_2$/NC were investigated by XAS, including X-ray absorption near-edge structure spectroscopy (XANES) and Fourier-transformed (FT) extended X-ray absorption fine structure spectroscopy (EXAFS). The Fe K pre-edges analyses show that the adsorption edge position of Fe in the catalyst is between FePc and $Fe_2O_3$, indicating the oxidation state of Fe (Figure 3a). The Fe K-edge FT EXAFS spectrum demonstrates a broad peak in the range of 1−2 Å and a peak at about 1.5 Å (Figure 3b).[6,57] No obvious peak at >2 Å is observed, indicating that


https://doi.org/10.1021/acsomega.3c06005
ACS Omega 2023, 8, 41708−41717

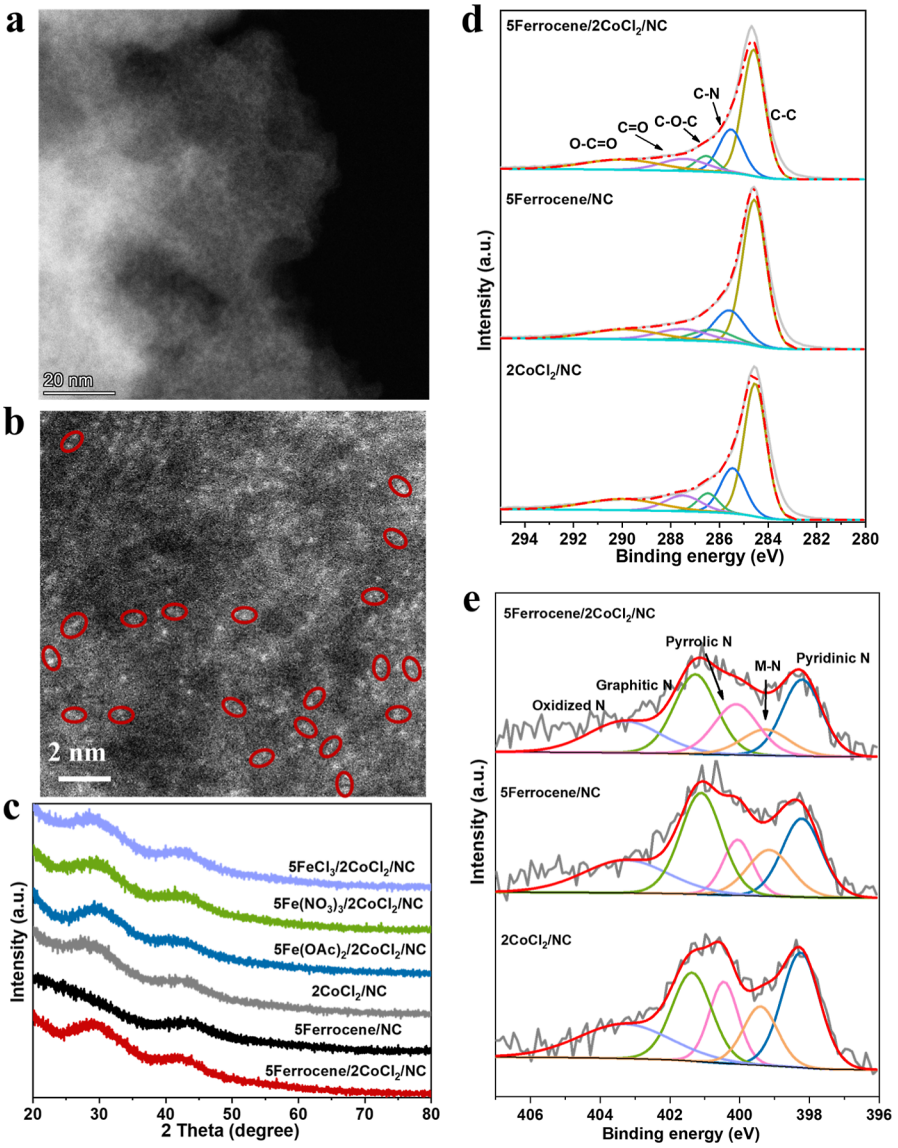


**Figure 2.** (a,b) AC-HAADF-STEM image of 5Ferrocene/$2CoCl_2$/NC, (c) XRD patterns of samples. High-resolution (d) C 1s and (e) N 1s XPS spectra of 5Ferrocene/$2CoCl_2$/NC, 5Ferrocene/NC, and $2CoCl_2$/NC.

the atomically dispersed Fe is the main Fe moieties in the 5Ferrocence/$2CoCl_2$/NC. The atomic Co structure in the catalyst is also analyzed by XANES and EXAFS spectra (Figure 3d,e). The coordination environments for Fe and Co were further analyzed by EXAFS fits using Fe−N/O and Co−N pathways (Figure 3c,f),[58,59] respectively. The fitting parameters are summarized in Table S4. The results indicate the $FeN_4$−$O_2$ moiety and Co−$N_4$ coexist in the sample. Additionally, no Fe−Co coordination information is detected, suggesting that the Fe and Co atoms may be randomly dispersed on the NC support.

The ORR performance of the obtained catalysts was tested using an RDE technique in an $O_2$-saturated 0.5 M $H_2SO_4$ solution, with all potentials referenced to the RHE. The ORR performance of all Fe, Co DACs is better than that of NC (0.691 V). The 5Ferrocene/NC sample showed good catalytic activity toward the ORR with an onset potential ($E_{onset}$) of 0.83 V and a half-wave potential ($E_{1/2}$) of 0.758 V (Figure 4a). However, introducing Co atoms did not always result in Fe, Co DACs being more active than the Fe single-atom catalysts (SAC). Specifically, 5Ferrocene/$2CoCl_2$/NC and 5Fe$(OAc)_2$/$2CoCl_2$/NC exhibited enhanced ORR activity with higher $E_{1/2}$ values of 0.774 and 0.768 V, respectively. 5$FeCl_3$/$2CoCl_2$/NC showed activity similar to that of 5Ferrocene/NC, while 5Fe$(NO_3)_3$/$2CoCl_2$/NC had decreased ORR activity with an approximate 39 mV lower $E_{1/2}$ than that of 5Ferrocene/$2CoCl_2$/NC. Therefore, the Fe precursor plays an important role in the ORR activity of Fe−N−C materials.

To determine the role of the Co metal, we prepared Fe, Co DACs by increasing the amount of $CoCl_2$. As shown in Figures 4b and S7, the ORR activity of Fe, Co DACs did not significantly improve using a higher amount of $CoCl_2$. For Ferrocene and Fe$(OAc)_2$, a slight increase in activity was observed, while decreased activity was found for the $FeCl_3$ precursor. Thus, it is difficult to improve the performance of Fe, Co DACs by adjusting the amount of metal precursors. The selectivity of catalysts toward the ORR was assessed through tracking evaluated the formation of $H_2O_2$, which was monitored using an RRDE technique. The $H_2O_2$ yield of 5Ferrocene/$2CoCl_2$/NC was below 3% in the potential range


https://doi.org/10.1021/acsomega.3c06005
ACS Omega 2023, 8, 41708−41717

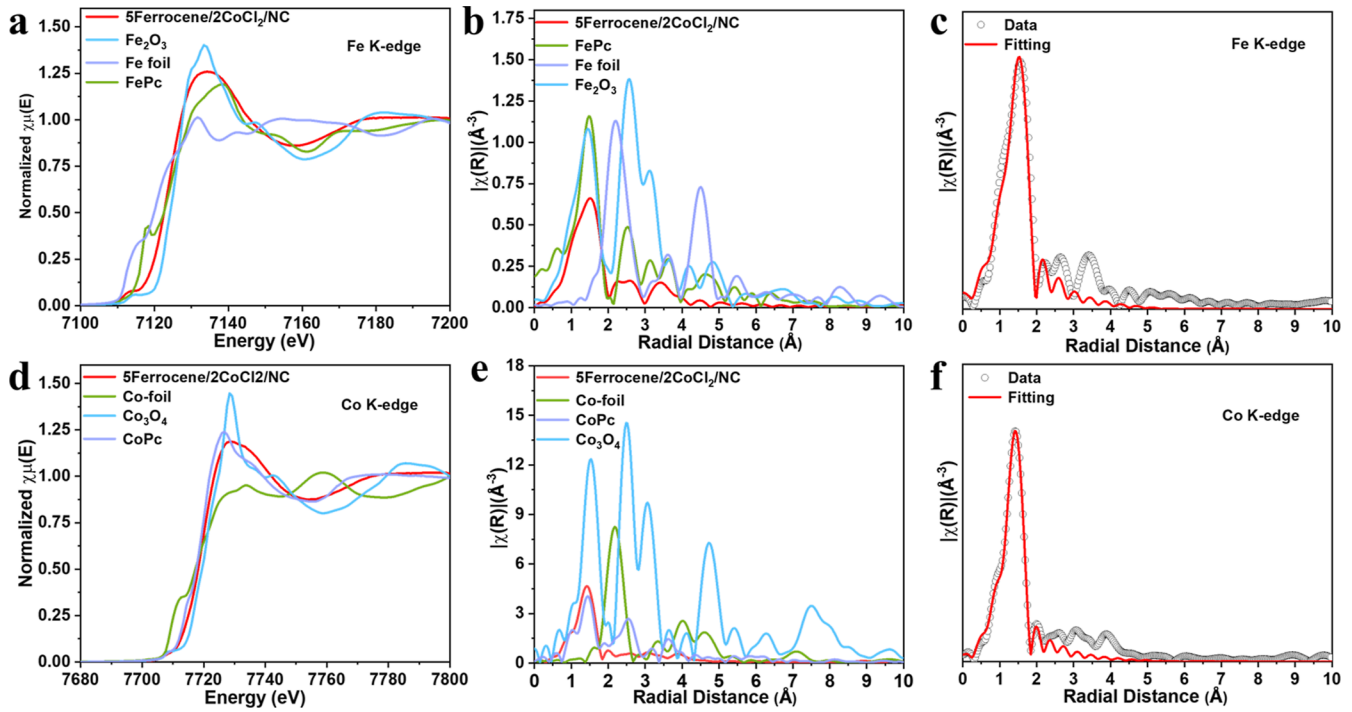


**Figure 3.** XAS analysis for 5Ferrocene/2$CoCl_2$/NC, with corresponding reference materials of Fe foil, Co foil, $Fe_2O_3$, $Co_3O_4$, FePc, and CoPc. K-edge XANES spectra of (a) Fe and (d) Co, EXAFS spectra of (b) Fe and (e) Co, and the corresponding fitting curves of (c) Fe and (f) Co.

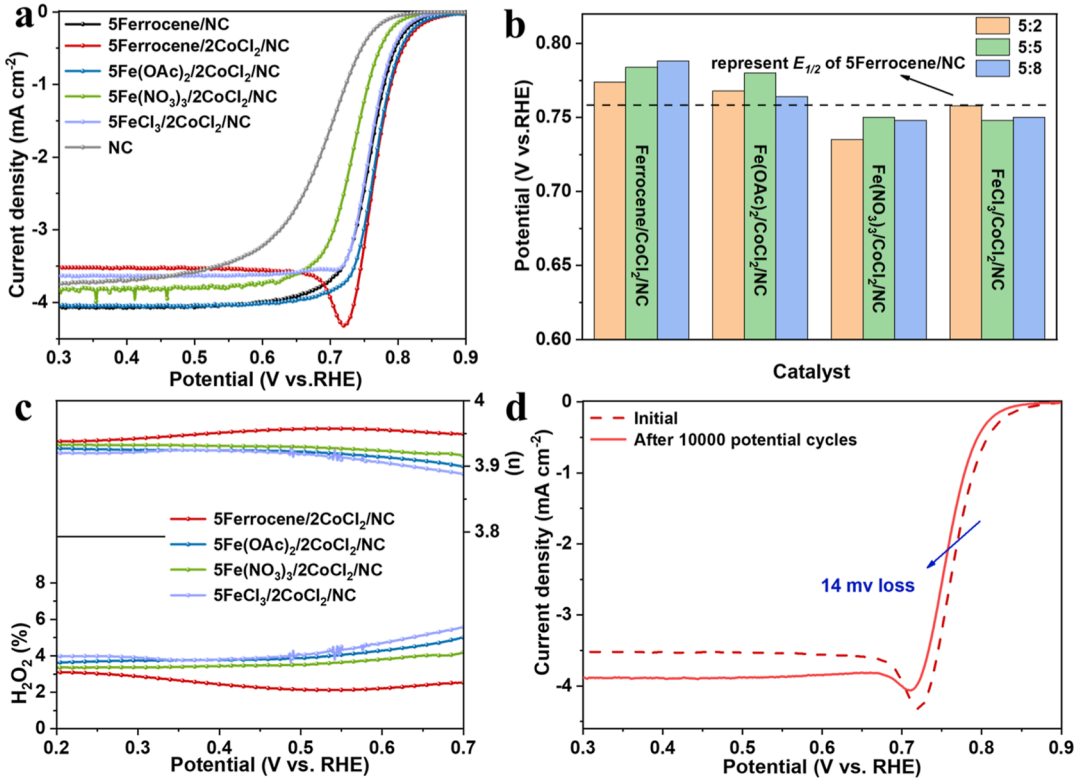


**Figure 4.** (a) RDE polarization curves of Fe, Co DACs, 5Ferrocene/NC, and NC; (b) $E_{1/2}$ values of Fe, Co DACs upon adjusting $CoCl_2$ contents; (c) $H_2O_2$ yields and electron transfer numbers; and (d) ORR polarization curves of 5Ferrocene/2$CoCl_2$/NC before and after 10,000 potential cycles.

from 0.2 to 0.7 V (Figure 4c). The electron transfer number was calculated to be ~4, indicating the four-electron process for the formation of $H_2O$. To evaluate its electrochemical durability, 5Ferrocene/2$CoCl_2$/NC was cycled from 0.6 to 1.0 V at 100 mV $s^{-1}$ in an $O_2$-saturated 0.5 M $H_2SO_4$ solution. After 10,000 potential cycles, the $E_{1/2}$ only decreased by 14 mV (Figure 4d) compared to that of 5Ferrocene/NC (Figure S8). The initial decrease should be attributed to the dematerializa-



https://doi.org/10.1021/acsomega.3c06005
ACS Omega 2023, 8, 41708−41717

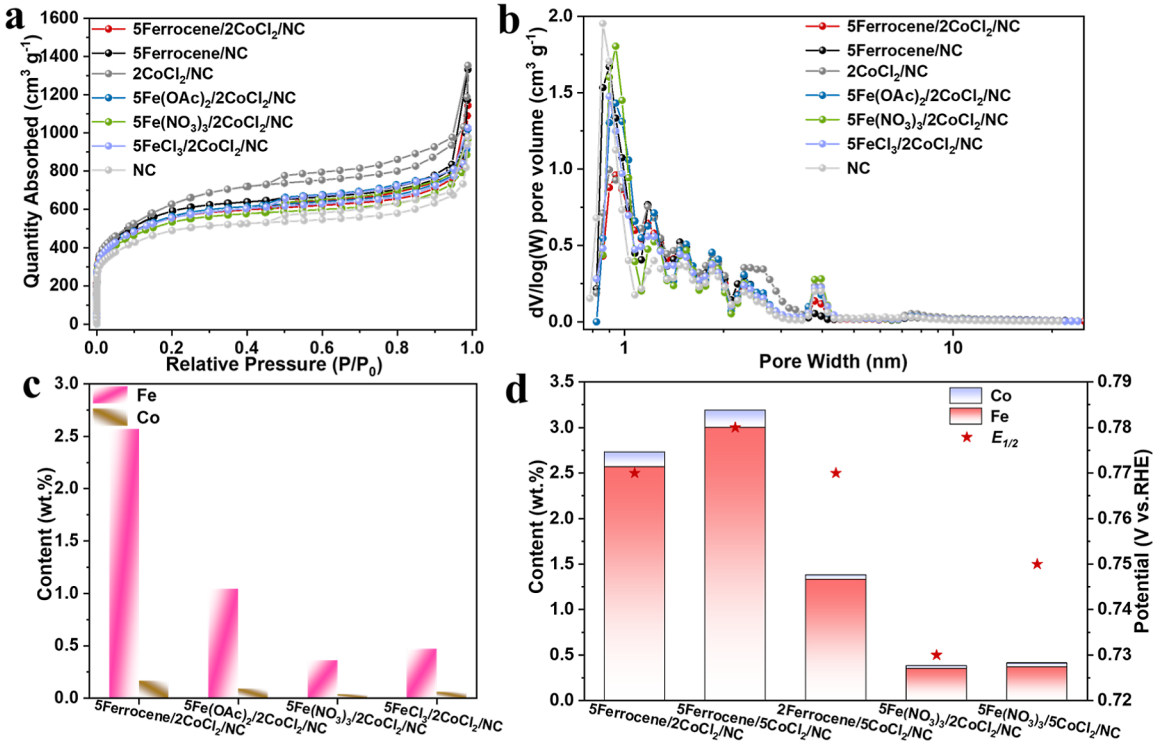


**Figure 5.** (a) $N_2$ adsorption/desorption isotherms and (b) pore size distributions of samples; (c) loadings of Fe and Co in 5Ferrocene/$2CoCl_2$/NC, 5Fe$(OAc)_2$/$2CoCl_2$/NC, 5Fe$(NO_3)_3$/$2CoCl_2$/NC, and 5$FeCl_3$/$2CoCl_2$/NC; and (d) values of Fe, Co contents, and $E_{1/2}$ for catalysts prepared using precursors of Ferrocene and Fe$(NO_3)_3$ with different Fe/Co ratios.

tion of unstable Fe active sites. Some clusters are observed from the AC-HAADF-STEM image after the stability test (Figure S9), indicating that unstable Fe atoms demetallized and formed the inactive Fe aggregates. It is well-known that the doped N acts as an anchoring site for stabilizing metal atoms.[52] Therefore, the XPS analysis was employed to investigate the change in the N structure. After the stability test, as seen in Figure S10 and Table S5, the N content of 5Ferrocene/$2CoCl_2$/NC was reduced from 3.37 to 1.85 at. %. The graphitic N, pyridinic-N, and M−N contents were also reduced, indicating that the decrease in the active sites contributed to the declined ORR performance. Interestingly, we found an increase in the limiting current. It is probably because of the improved mass transport of the catalyst. The $O_2$ dissolved in electrolyte can reach the three-phase boundary of catalysts.

In order to explore the role of metal precursors on the ORR activity, we then examined the porous property of samples. The textural porosities of the catalysts were analyzed by $N_2$ adsorption−desorption analysis. All samples exhibited typical type IV isotherms with H2 hysteresis loops. The absorbed volume increases quickly at a low relative pressure, revealing the existence of micropores. The coexistence of micro- and mesopores demonstrates the hierarchical porous feature (Figure 5a). Based on the pore size distributions (Figure 5b), all samples demonstrate similar micro- and mesoporous structures. Additionally, the BET surface areas of micro- and mesopores are also similar (Table S6). One can conclude that the metal precursors have no obvious influence on the porous structure of final products.

Then, we investigated the thermal stability of metal precursors by TGA. It was observed that less weight loss occurred when using the ferrocene and $CoCl_2$ precursors, whereas the Fe$(NO_3)_3$ sample exhibited a significant loss (Figure S11). The high thermal stability of the metal precursors may protect the metals from oxidation at low temperatures, thereby minimizing the formation of metal aggregates.[60]

The site density ($SD_{mass}$) of the catalysts was measured by the in situ electrochemical nitrite poisoning method. As shown in Figure S12 and Table S7, 5Ferrocene/$2CoCl_2$/NC, 5Fe$(OAc)_2$/$2CoCl_2$/NC, 5$FeCl_3$/$2CoCl_2$/NC, and 5Fe-$(NO_3)_3$/$2CoCl_2$/NC with the site density decreasing also showed decreased ORR activities. Although 5Ferrocene/$2CoCl_2$/NC showed the highest $SD_{mass}$ ($4.88 \times 10^{18}$ site $g^{-1}$), which was 5.4-times higher than that of 5Fe$(NO_3)_3$/$2CoCl_2$/NC ($8.92 \times 10^{17}$ site $g^{-1}$), it was still much worse than that in the reported work[6] ($4.57 \times 10^{20}$ site $g^{-1}$), which led to an ordinary ORR performance compared to other catalysts in acidic solution (Table S8).

Next, we measured the loadings of Fe and Co in a series of Fe, Co DACs using an inductively coupled plasma optical emission spectrometer. The Fe, Co DAC with the highest Fe and Co loadings (2.57 wt % Fe and 0.16 wt % Co) was found to be 5Ferrocene/$2CoCl_2$/NC, while the one with the lowest metal loadings was observed (0.35 wt % Fe and 0.03 wt % Co) to be 5Fe$(NO_3)_3$/$2CoCl_2$/NC (Figure 5c). The best ORR activity was observed in 5Ferrocene/$5CoCl_2$/NC, which can be attributed to both high Fe and Co contents (Figure 5d). Interestingly, we found that Fe always dominated the metal content in Fe, Co DACs. Although we attempted to increase the Co loading by using more $CoCl_2$, both metal contents decreased in 2Ferrocene/$5CoCl_2$/NC (1.33 wt % Fe and 0.05 wt % Co), resulting in a decline in activity. This suggests that it is challenging to improve both Fe and Co loadings by adjusting the metal precursors. Therefore, we predict that the metal


https://doi.org/10.1021/acsomega.3c06005
ACS Omega 2023, 8, 41708−41717

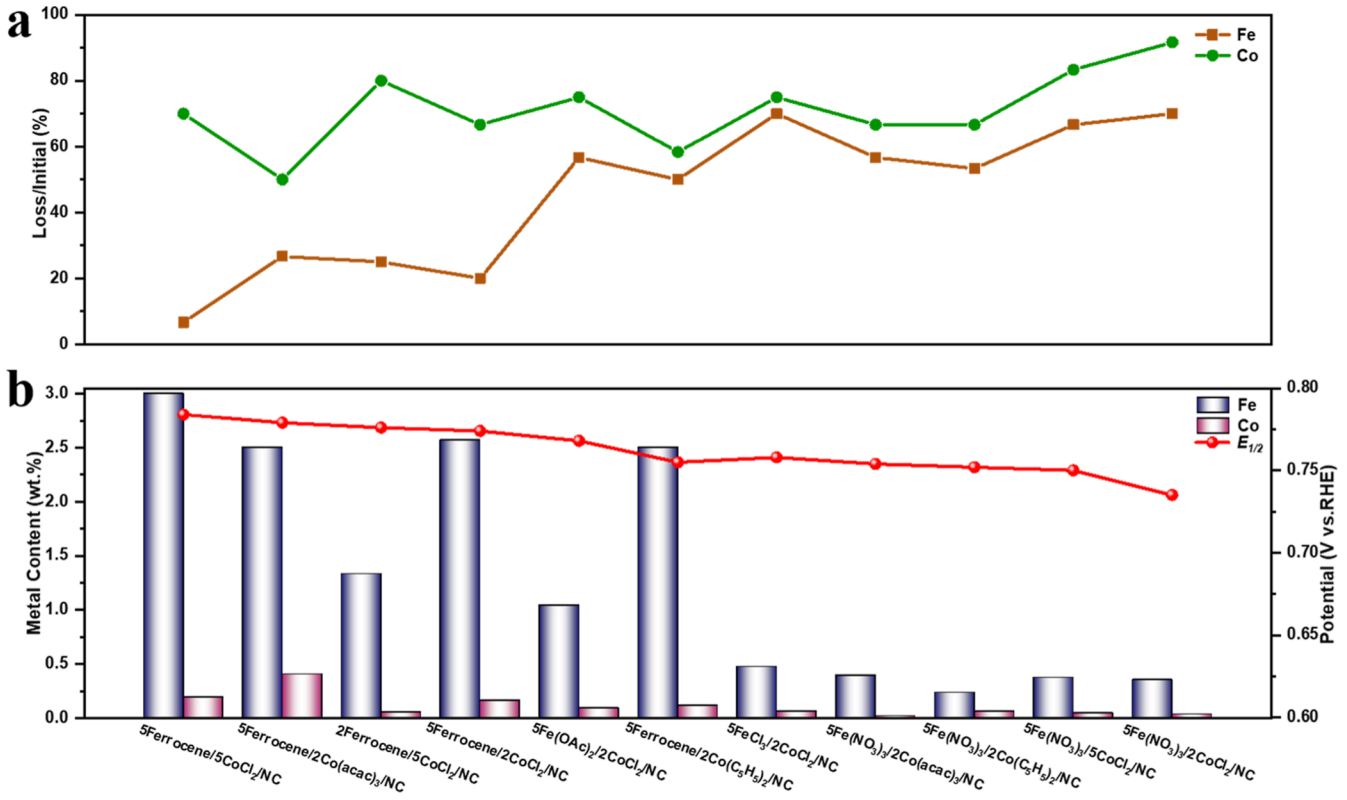


**Figure 6.** (a) Loss of precursors after the washing process, and (b) corresponding loading amounts of Fe and Co and $E_{1/2}$ of samples containing different types, contents, and ratios of Fe and Co precursors.

loading strongly depends on the adsorption ability of metal precursors on the NC supports.

Interestingly, Mehmood and co-workers[61] demonstrated that Fe active sites are more favored to be formed on a nitrogen-doped carbon matrix than Co, leading to a much higher content of Fe (e.g., 0.03 wt % Co versus 0.46 wt % Fe). The chemistry coordination between different metal precursors may play a key role in the formation of active sites on the nitrogen-doped carbon matrix. Inspired by this work, we further comprehensively investigate the difference of adsorption ability of NC toward various combinations of Fe and Co precursors. The loss of metal precursors from the NC supports after using a centrifugal washing process was measured by using an atomic absorption spectrometry (AAS) method. We considered a series of combinations based on different metal precursors and their initial molar ratios. Digital photographs of the supernatant color for different samples can be seen in Figure S13. The centrifugal supernatant displayed the obvious color of Fe precursors, such as samples with $Fe(NO_3)_3$ and $FeCl_3$. The initial amounts and loss of Fe and Co precursors are summarized in Table S9. As shown in Figure 6a, a significant loss occurred for all metal precursors after the washing process, indicating the difficulty of the adsorption−annealing method for synthesizing dense SACs. Specifically, for the initial ratios of 5:2 for Fe and Co precursors, the ferrocene showed only a 20% loss, while $Fe(OAc)_2$ had a 57% loss and $FeCl_3$ and $Fe(NO_3)_3$ had a 70% loss.

When ferrocene is used, $Co(acac)_3$ displayed the best adsorption on the NC with the smallest loss of 50%. Importantly, 50−90% of Co precursors were lost, which is more than Fe precursors, indicating possible adsorption competition between Fe and Co precursors. It is worth noting that the Fe precursors always win this competition. When the initial ratio of Fe and Co precursors is increased from 5:2 to 2:5, the residual Co precursors are still much lower than that of Fe precursors. As a result, the Fe loadings in the final catalysts are much higher than that of Co. Among these combinations, ferrocene and $CoCl_2$ are the best compositions for synthesizing Fe, Co DACs. The adsorption property of metal precursors greatly influences the final metal loading (Table S10), which in turn affects the ORR performance (Figures 6b and S14). First, the ORR activity of Fe, Co DACs is mainly determined by the Fe loading due to its higher intrinsic activity than that of Co. Second, increasing the Co loading can further improve the ORR activity. Lastly, 5ferrocence/$5CoCl_2$/NC exhibits the best ORR activity due to its high Fe and Co contents. In order to confirm the existence of adsorption competition between Fe and Co precursors, we synthesized various carbon materials, including N-doped graphene (NG), ZIF-8-derived NC without using NaCl (NC-1000), and ZIF-8-derived NC with NaCl annealed at 1000 °C [NC(Na)−1000] (see details of preparation in the Supporting Information). The adsorption behaviors of Fe and Co on these carbon supports were studied. Figure S15 shows the adsorption behaviors of Fe and Co on various carbon supports. The results consistently demonstrated that Fe precursors have a higher affinity for adsorption compared to Co precursors in most cases (Figure S15 and Table S11). Interestingly, a combination of ferrocene and $CoCl_2$ exhibited the most favorable adsorption behavior on the carbon supports. These findings further confirm the dominance of Fe precursors in the adsorption competition and shed light on the potential benefits of using specific combinations of precursors for effective DAC synthesis on carbon materials.


https://doi.org/10.1021/acsomega.3c06005
ACS Omega 2023, 8, 41708−41717

## CONCLUSIONS

In summary, we have demonstrated various Fe, Co DACs using adsorption−annealing methods. A series of combinations of Fe and Co precursors were studied based on different metal precursors and their initial mole ratios. The correlation of the resulting Fe and Co loadings in the final samples and ORR activity has been established. The adsorption ability of metal precursors has been demonstrated to be responsible for the difference in Fe and Co loading in final catalysts. Surprisingly, the Fe precursors always win the adsorption competitions, leading to a much higher loading than that of Co. The results suggested that maintaining the ratio of Fe and Co precursors, for instance, without the washing process, may help adjust the Fe and Co loadings. Unfortunately, it usually causes serious metal aggregates rather than isolated atoms on the NC support (Figure S16). The findings of this work will stimulate the exploration of highly active, controllable nitrogen-doped carbon-supporting DACs and their electrochemical properties.

## ASSOCIATED CONTENT

### Supporting Information

The Supporting Information is available free of charge at https://pubs.acs.org/doi/10.1021/acsomega.3c06005.

Experimental Section, characterizations such as SEM, TEM, and HR-TEM images, XPS spectral information, BET results, ICP-OES and AAS results, and electrochemical test results (PDF)

## AUTHOR INFORMATION


### Corresponding Authors

**Guangbo Chen** − *Faculty of Chemistry and Food Chemistry &; Center for Advancing Electronics Dresden (cfaed), Technische Universität Dresden, Dresden 01062, Germany;* orcid.org/0000-0003-1927-3642; Email: guangbo.chen@tu-dresden.de

**Yazhou Zhou** − *School of Materials Science and Engineering, Jiangsu University, Zhenjiang 212013 Jiangsu, China; Max Planck Institute for Polymer Research, Mainz 55128, Germany;* orcid.org/0000-0002-0446-2291; Email: yazhou@ujs.edu.cn

### Authors

**Xiu Zhu** − *School of Materials Science and Engineering, Jiangsu University, Zhenjiang 212013 Jiangsu, China*

**Genlin Liu** − *Institute of Functional Nano & Soft Materials (FUNSOM), Soochow University, Suzhou 215123 Jiangsu, China*

**Xiafang Tao** − *School of Materials Science and Engineering, Jiangsu University, Zhenjiang 212013 Jiangsu, China; Max Planck Institute for Polymer Research, Mainz 55128, Germany*

**Pengwei Huang** − *School of Materials Science and Engineering, Jiangsu University, Zhenjiang 212013 Jiangsu, China*

**Qing Wang** − *Institute for Catalysis, Hokkaido University, Sapporo 001-0021, Japan*

**Juan Yang** − *School of Materials Science and Engineering, Jiangsu University, Zhenjiang 212013 Jiangsu, China;* orcid.org/0000-0003-0118-7084

**Liang Zhang** − *Institute of Functional Nano & Soft Materials (FUNSOM), Soochow University, Suzhou 215123 Jiangsu, China;* orcid.org/0000-0002-3446-3172

Complete contact information is available at: https://pubs.acs.org/10.1021/acsomega.3c06005


### Notes

The authors declare no competing financial interest.

## ACKNOWLEDGMENTS

This work was financially supported by the National Natural Science Foundation of China (grant nos. 51702129 and 51972150), the DFG (514772236), and the Max Planck Society. The authors thank the Shanghai Synchrotron Radiation Facility (SSRF) (beamline 11B) and Beijing Synchrotron Radiation Facility (BSRF) (beamline 1W1B) for the allocation of synchrotron beamtime.

## REFERENCES


(1) Li, J.; Sougrati, M. T.; Zitolo, A.; Ablett, J. M.; Oğuz, I. C.; Mineva, T.; Matanovic, I.; Atanassov, P.; Huang, Y.; Zenyuk, I.; Di Cicco, A.; Kumar, K.; Dubau, L.; Maillard, F.; Dražić, G.; Jaouen, F. Identification of durable and non-durable $FeN_x$ sites in Fe-N-C materials for proton exchange membrane fuel cells. *Nat. Catal.* **2020**, *4*, 10−19.

(2) Qu, Q.; Ji, S.; Chen, Y.; Wang, D.; Li, Y. Design and structural engineering of single-atomic-site catalysts for acidic oxygen reduction reaction. *Trends Chem.* **2021**, *3*, 954−968.

(3) Zhang, H.; Chung, H. T.; Cullen, D. A.; Wagner, S.; Kramm, U. I.; More, K. L.; Zelenay, P.; Wu, G. High-performance fuel cell cathodes exclusively containing atomically dispersed iron active sites. *Energy Environ. Sci.* **2019**, *12*, 2548−2558.

(4) Wei, X.; Song, S.; Cai, W.; Luo, X.; Jiao, L.; Fang, Q.; Wang, X.; Wu, N.; Luo, Z.; Wang, H.; Zhu, Z.; Li, J.; Zheng, L.; Gu, W.; Song, W.; Guo, S.; Zhu, C. Tuning the spin state of Fe single atoms by Pd nanoclusters enables robust oxygen reduction with dissociative pathway. *Chem.* **2023**, *9*, 181−197.

(5) Jiao, L.; Li, J.; Richard, L. L.; Sun, Q.; Stracensky, T.; Liu, E.; Sougrati, M. T.; Zhao, Z.; Yang, F.; Zhong, S.; Xu, H.; Mukerjee, S.; Huang, Y.; Cullen, D. A.; Park, J. H.; Ferrandon, M.; Myers, D. J.; Jaouen, F.; Jia, Q. Chemical vapour deposition of Fe-N-C oxygen reduction catalysts with full utilization of dense Fe-$N_4$ sites. *Nat. Mater.* **2021**, *20*, 1385−1391.

(6) Zhou, Y.; Chen, G.; Wang, Q.; Wang, D.; Tao, X.; Zhang, T.; Feng, X.; Müllen, K. Fe-N-C Electrocatalysts with Densely Accessible $FeN_4$ Sites for Efficient Oxygen Reduction Reaction. *Adv. Funct. Mater.* **2021**, *31*, 2102420.

(7) Liu, F.; Shi, L.; Lin, X.; Yu, D.; Zhang, C.; Xu, R.; Liu, D.; Qiu, J.; Dai, L. Site-density engineering of single-atomic iron catalysts for high-performance proton exchange membrane fuel cells. *Appl. Catal., B* **2022**, *302*, 120860.

(8) Wan, X.; Shui, J. Exploring Durable Single-Atom Catalysts for Proton Exchange Membrane Fuel Cells. *ACS Energy Lett.* **2022**, *7*, 1696−1705.

(9) Xiao, M.; Chen, Y.; Zhu, J.; Zhang, H.; Zhao, X.; Gao, L.; Wang, X.; Zhao, J.; Ge, J.; Jiang, Z.; Chen, S.; Liu, C.; Xing, W. Climbing the Apex of the ORR Volcano Plot via Binuclear Site Construction: Electronic and Geometric Engineering. *J. Am. Chem. Soc.* **2019**, *141*, 17763−17770.

(10) Lu, R.; Quan, C.; Zhang, C.; He, Q.; Liao, X.; Wang, Z.; Zhao, Y. Establishing a theoretical insight for penta-coordinated iron-nitrogen-carbon catalysts toward oxygen reaction. *Nano Res.* **2022**, *15*, 6067−6075.

(11) Choi, C. H.; Lim, H.-K.; Chung, M. W.; Chon, G.; Ranjbar Sahraie, N.; Altin, A.; Sougrati, M.-T.; Stievano, L.; Oh, H. S.; Park, E. S.; Luo, F.; Strasser, P.; Dražić, G.; Mayrhofer, K. J. J.; Kim, H.; Jaouen, F. The Achilles' heel of iron-based catalysts during oxygen reduction in an acidic medium. *Energy Environ. Sci.* **2018**, *11*, 3176−3182.

(12) Kumar, K.; Gairola, P.; Lions, M.; Ranjbar-Sahraie, N.; Mermoux, M.; Dubau, L.; Zitolo, A.; Jaouen, F.; Maillard, F. Physical and Chemical Considerations for Improving Catalytic Activity and Stability of Non-Precious-Metal Oxygen Reduction Reaction Catalysts. *ACS Catal.* **2018**, *8*, 11264−11276.
(13) Jeong, H.; Shin, S.; Lee, H. Heterogeneous Atomic Catalysts Overcoming the Limitations of Single-Atom Catalysts. *ACS Nano* **2020**, *14*, 14355−14374.
(14) Zhou, Y.; Lu, R.; Tao, X.; Qiu, Z.; Chen, G.; Yang, J.; Zhao, Y.; Feng, X.; Mullen, K. Boosting Oxygen Electrocatalytic Activity of Fe-N-C Catalysts by Phosphorus Incorporation. *J. Am. Chem. Soc.* **2023**, *145*, 3647−3655.
(15) Tao, X.; Lu, R.; Ni, L.; Gridin, V.; Al-Hilfi, S. H.; Qiu, Z.; Zhao, Y.; Kramm, U. I.; Zhou, Y.; Mullen, K. Facilitating the acidic oxygen reduction of Fe-N-C catalysts by fluorine-doping. *Mater. Horiz.* **2022**, *9*, 417−424.
(16) Razmjooei, F.; Singh, K. P.; Yang, D.-S.; Cui, W.; Jang, Y. H.; Yu, J.-S. Fe-Treated Heteroatom (S/N/B/P)-Doped Graphene Electrocatalysts for Water Oxidation. *ACS Catal.* **2017**, *7*, 2381−2391.
(17) Li, Z.; Yan, Y.; Liu, M.; Qu, Z.; Yue, Y.; Mao, T.; Zhao, S.; Liu, M.; Lin, Z. Robust ring-opening reaction via asymmetrically coordinated Fe single atoms scaffolded by spoke-like mesoporous carbon nanospheres. *Proc. Natl. Acad. Sci. U.S.A.* **2023**, *120*, No. e2218261120.
(18) Wei, X.; Luo, X.; Wu, N.; Gu, W.; Lin, Y.; Zhu, C. Recent advances in synergistically enhanced single-atomic site catalysts for boosted oxygen reduction reaction. *Nano Energy* **2021**, *84*, 105817.
(19) Mehmood, A.; Gong, M.; Jaouen, F.; Roy, A.; Zitolo, A.; Khan, A.; Sougrati, M.-T.; Primbs, M.; Bonastre, A. M.; Fongalland, D.; Drazic, G.; Strasser, P.; Kucernak, A. High loading of single atomic iron sites in Fe-NC oxygen reduction catalysts for proton exchange membrane fuel cells. *Nat. Catal.* **2022**, *5*, 311−323.
(20) Zhou, Y.; Tao, X.; Chen, G.; Lu, R.; Wang, D.; Chen, M.-X.; Jin, E.; Yang, J.; Liang, H.-W.; Zhao, Y.; Feng, X.; Narita, A.; Müllen, K. Multilayer stabilization for fabricating high-loading single-atom catalysts. *Nat. Commun.* **2020**, *11*, 5892.
(21) Jiang, M.; Wang, F.; Yang, F.; He, H.; Yang, J.; Zhang, W.; Luo, J.; Zhang, J.; Fu, C. Rationalization on high-loading iron and cobalt dual metal single atoms and mechanistic insight into the oxygen reduction reaction. *Nano Energy* **2022**, *93*, 106793.
(22) Cai, H.; Zhang, G.; Zhang, X.; Chen, B.; Lu, Z.; Xu, H.; Gao, R.; Shi, C. Engineering the Local Coordination Environment and Density of $FeN_4$ Sites by Mn Cooperation for Electrocatalytic Oxygen Reduction. *Small* **2022**, *18*, No. e2200911.
(23) Wang, Z.; Jin, H.; Meng, T.; Liao, K.; Meng, W.; Yang, J.; He, D.; Xiong, Y.; Mu, S. Fe, Cu-Coordinated ZIF-Derived Carbon Framework for Efficient Oxygen Reduction Reaction and Zinc-Air Batteries. *Adv. Funct. Mater.* **2018**, *28*, 1802596.
(24) Zhang, X.; Li, Y.; Jiang, M.; Wei, J.; Ding, X.; Zhu, C.; He, H.; Lai, H.; Shi, J. Engineering the coordination environment in atomic Fe/Ni dual-sites for efficient oxygen electrocatalysis in Zn-air and Mg-air batteries. *Chem. Eng. J.* **2021**, *426*, 130758.
(25) Yan, Y.; Cheng, H.; Qu, Z.; Yu, R.; Liu, F.; Ma, Q.; Zhao, S.; Hu, H.; Cheng, Y.; Yang, C.; Li, Z.; Wang, X.; Hao, S.; Chen, Y.; Liu, M. Recent progress on the synthesis and oxygen reduction applications of Fe-based single-atom and double-atom catalysts. *J. Mater. Chem. A* **2021**, *9*, 19489−19507.
(26) Pedersen, A.; Barrio, J.; Li, A.; Jervis, R.; Brett, D. J. L.; Titirici, M. M.; Stephens, I. E. L. Dual-Metal Atom Electrocatalysts: Theory, Synthesis, Characterization, and Applications. *Adv. Energy Mater.* **2021**, *12*, 2102715.
(27) Tamtaji, M.; Peng, Q.; Liu, T.; Zhao, X.; Xu, Z.; Galligan, P. R.; Hossain, M. D.; Liu, Z.; Wong, H.; Liu, H.; Amine, K.; Zhu, Y.; Goddard, W. A., III; Wu, W.; Luo, Z. Non-bonding interaction of dual atom catalysts for enhanced oxygen reduction reaction. *Nano Energy* **2023**, *108*, 108218.
(28) Shan, J.; Ye, C.; Jiang, Y.; Jaroniec, M.; Zheng, Y.; Qiao, S. Metal-metal interactions in correlated single-atom catalysts. *Sci. Adv.* **2022**, *8*, No. eabo0762.
(29) Leng, K.; Zhang, J.; Wang, Y.; Li, D.; Bai, L.; Shi, J.; Li, X.; Zheng, L.; Bai, J.; Qu, Y. Interfacial Cladding Engineering Suppresses Atomic Thermal Migration to Fabricate Well-Defined Dual-Atom Electrocatalysts. *Adv. Funct. Mater.* **2022**, *32*, 2205637.
(30) Zhang, L.; Feng, J.; Liu, S.; Tan, X.; Wu, L.; Jia, S.; Xu, L.; Ma, X.; Song, X.; Ma, J.; Sun, X.; Han, B. Atomically Dispersed Ni-Cu Catalysts for pH-Universal $CO_2$ Electroreduction. *Adv. Mater.* **2023**, *35*, No. e2209590.
(31) Wang, J.; Huang, Z.; Liu, W.; Chang, C.; Tang, H.; Li, Z.; Chen, W.; Jia, C.; Yao, T.; Wei, S.; Wu, Y.; Li, Y. Design of N-Coordinated Dual-Metal Sites: A Stable and Active Pt-Free Catalyst for Acidic Oxygen Reduction Reaction. *J. Am. Chem. Soc.* **2017**, *139*, 17281−17284.
(32) Han, A.; Sun, W.; Wan, X.; Cai, D.; Wang, X.; Li, F.; Shui, J.; Wang, D. Construction of $Co_4$ Atomic Clusters to Enable Fe-$N_4$ Motifs with Highly Active and Durable Oxygen Reduction Performance. *Angew. Chem., Int. Ed.* **2023**, *62*, No. e202303185.
(33) Wang, Y.; Park, B. J.; Paidi, V. K.; Huang, R.; Lee, Y.; Noh, K.-J.; Lee, K.-S.; Han, J. W. Precisely Constructing Orbital Coupling-Modulated Dual-Atom Fe Pair Sites for Synergistic $CO_2$ Electroreduction. *ACS Energy Lett.* **2022**, *7*, 640−649.
(34) Zhu, P.; Xiong, X.; Wang, X.; Ye, C.; Li, J.; Sun, W.; Sun, X.; Jiang, J.; Zhuang, Z.; Wang, D.; Li, Y. Regulating the $FeN_4$ Moiety by Constructing Fe-Mo Dual-Metal Atom Sites for Efficient Electrochemical Oxygen Reduction. *Nano Lett.* **2022**, *22*, 9507−9515.
(35) Lu, X. F.; Chen, Y.; Wang, S.; Gao, S.; Lou, X. W. D. Interfacing Manganese Oxide and Cobalt in Porous Graphitic Carbon Polyhedrons Boosts Oxygen Electrocatalysis for Zn-Air Batteries. *Adv. Mater.* **2019**, *31*, No. e1902339.
(36) Liang, Z.; Song, L.; Sun, M.; Huang, B.; Du, Y. Tunable CO/$H_2$ ratios of electrochemical reduction of $CO_2$ through the Zn-Ln dual atomic catalysts. *Sci. Adv.* **2021**, *7*, No. eabl4915.
(37) Zhu, Z.; Yin, H.; Wang, Y.; Chuang, C. H.; Xing, L.; Dong, M.; Lu, Y. R.; Casillas-Garcia, G.; Zheng, Y.; Chen, S.; Dou, Y.; Liu, P.; Cheng, Q.; Zhao, H. Coexisting Single-Atomic Fe and Ni Sites on Hierarchically Ordered Porous Carbon as a Highly Efficient ORR Electrocatalyst. *Adv. Mater.* **2020**, *32*, No. e2004670.
(38) Zeng, Z.; Gan, L. Y.; Bin Yang, H.; Su, X.; Gao, J.; Liu, W.; Matsumoto, H.; Gong, J.; Zhang, J.; Cai, W.; Zhang, Z.; Yan, Y.; Liu, B.; Chen, P. Orbital coupling of hetero-diatomic nickel-iron site for bifunctional electrocatalysis of $CO_2$ reduction and oxygen evolution. *Nat. Commun.* **2021**, *12*, 4088.
(39) Yan, Y.; Liang, S.; Wang, X.; Zhang, M.; Hao, S. M.; Cui, X.; Li, Z.; Lin, Z. Robust wrinkled $MoS_2$/N-C bifunctional electrocatalysts interfaced with single Fe atoms for wearable zinc-air batteries. *Proc. Natl. Acad. Sci. U.S.A.* **2021**, *118*, 40e2110036118.
(40) Zhu, Y.; Sokolowski, J.; Song, X.; He, Y.; Mei, Y.; Wu, G. Engineering Local Coordination Environments of Atomically Dispersed and Heteroatom-Coordinated Single Metal Site Electrocatalysts for Clean Energy-Conversion. *Adv. Energy Mater.* **2019**, *10*, 1902844.
(41) Zang, Y.; Mi, C.; Wang, R.; Chen, H.; Peng, P.; Xiang, Z.; Zang, S. Q.; Mak, T. C. W. Pyrolysis-Free Synthesized Catalyst towards Acidic Oxygen Reduction by Deprotonation. *Angew. Chem., Int. Ed.* **2021**, *60*, 20865−20871.
(42) Ouyang, C.; Zheng, L.; Zhang, Q.; Wang, X. A Simple Preheating-Pyrolysis Strategy Leading to Superior Oxygen Reduction Reaction Activity in Fe-N/Carbon Black. *Adv. Mater.* **2022**, *34*, No. e2205372.
(43) He, T.; Santiago, A. R. P.; Kong, Y.; Ahsan, M. A.; Luque, R.; Du, A.; Pan, H. Atomically Dispersed Heteronuclear Dual-Atom Catalysts: A New Rising Star in Atomic Catalysis. *Small* **2021**, *18*, 2106091.
(44) He, J.; Zheng, T.; Wu, D.; Zhang, S.; Gu, M.; He, Q. Insights into the Determining Effect of Carbon Support Properties on Anchoring Active Sites in Fe-N-C Catalysts toward the Oxygen Reduction Reaction. *ACS Catal.* **2022**, *12*, 1601−1613.
(45) Wu, Y.; Ye, C.; Yu, L.; Liu, Y.; Huang, J.; Bi, J.; Xue, L.; Sun, J.; Yang, J.; Zhang, W.; Wang, X.; Xiong, P.; Zhu, J. Soft template-


https://doi.org/10.1021/acsomega.3c06005
*ACS Omega* 2023, 8, 41708−41717

directed interlayer confinement synthesis of a Fe-Co dual single-atom catalyst for Zn-air batteries. *Energy Storage Mater.* **2022**, *45*, 805−813.
(46) Zhang, L.; Fischer, J.; Jia, Y.; Yan, X.; Xu, W.; Wang, X.; Chen, J.; Yang, D.; Liu, H.; Zhuang, L.; Hankel, M.; Searles, D. J.; Huang, K.; Feng, S.; Brown, C. L.; Yao, X. Coordination of Atomic Co-Pt Coupling Species at Carbon Defects as Active Sites for Oxygen Reduction Reaction. *J. Am. Chem. Soc.* **2018**, *140*, 10757−10763.
(47) Nandan, R.; Pandey, P.; Gautam, A.; Bisen, O. Y.; Chattopadhyay, K.; Titirici, M. M.; Nanda, K. K. Atomic Arrangement Modulation in CoFe Nanoparticles Encapsulated in N-Doped Carbon Nanostructures for Efficient Oxygen Reduction Reaction. *ACS Appl. Mater. Interfaces* **2021**, *13*, 3771−3781.
(48) Malko, D.; Kucernak, A.; Lopes, T. In situ electrochemical quantification of active sites in Fe-N/C non-precious metal catalysts. *Nat. Commun.* **2016**, *7*, 13285.
(49) Wei, X.; Song, S.; Wu, N.; Luo, X.; Zheng, L.; Jiao, L.; Wang, H.; Fang, Q.; Hu, L.; Gu, W.; Song, W.; Zhu, C. Synergistically enhanced single-atomic site Fe by $Fe_3C$@C for boosted oxygen reduction in neutral electrolyte. *Nano Energy* **2021**, *84*, 105840.
(50) Song, Q.; Bian, W.; Yue, Q.; Zhang, B.; Guo, T.; Bai, J.; Wang, Z.; Tan, W.; Zhou, B. Self-etched bimetallic hybrid derived cobalt/zinc dual-sites coordinated N, P-codoped hollow carbon polyhedron for efficient oxygen reduction reaction. *Mater. Today Adv.* **2023**, *17*, 100334.
(51) Chen, Y.; Qiao, S.; Tang, Y.; Du, Y.; Zhang, D.; Wang, W.; Zhang, H.; Sun, X.; Liu, C. Double-Faced Atomic-Level Engineering of Hollow Carbon Nanofibers as Free-Standing Bifunctional Oxygen Electrocatalysts for Flexible Zn-Air Battery. *ACS Nano* **2022**, *16*, 15273−15285.
(52) Li, Z.; Yu, H.; Zhang, Y.; Wu, D.; Bai, Y.; Liu, S.; Zhao, H. An attempt to confirm the contribution to ORR activity of different N-species in M-NC (M = Fe, Co, Ni) catalysts with XPS analysis. *Chem. Commun.* **2023**, *59*, 4535−4538.
(53) Xu, M. H.; Wang, Y. H.; He, W. H.; Li, X. D.; Meng, X. H.; Li, C. C.; Li, X. T.; Kong, Q. H.; Shen, L. F.; Zhang, J.; Zhang, X.; Xin, S.; Guo, Y. G. A N-Rich porous carbon nanocube anchored with Co/Fe dual atoms: an efficient bifunctional catalytic host for Li-S batteries. *Mater. Chem. Front.* **2022**, *6*, 2095−2102.
(54) Zhou, Y.; Liu, Y.; Wang, Z.; Li, C.; Wang, Z.; Zhang, S.; Deng, C. Fe-Co dual atomic doublets on N, P codoped carbon as active sites in the framework of heterostructured hollow fibers towards high-performance flexible Zn-Air battery. *Energy Storage Mater.* **2023**, *59*, 102772.
(55) Zhao, C.; Liu, J.; Wang, J.; Wang, C.; Guo, X.; Li, X.; Chen, X.; Song, Li.; Li, B.; Zhang, Q. A clicking confinement strategy to fabricate transition metal single-atom sites for bifunctional oxygen electrocatalysis. *Sci. Adv.* **2022**, *8*, No. eabn5091.
(56) Pei, Z.; Lu, X. F.; Zhang, H.; Li, Y.; Luan, D.; Lou, X. W. D. Highly Efficient Electrocatalytic Oxygen Evolution Over Atomically Dispersed Synergistic Ni/Co Dual Sites. *Angew. Chem., Int. Ed.* **2022**, *61*, No. e202207537.
(57) Wang, Z.; Jin, X.; Zhu, C.; Liu, Y.; Tan, H.; Ku, R.; Zhang, Y.; Zhou, L.; Liu, Z.; Hwang, S. J.; Fan, H. J. Atomically Dispersed $Co_2$-$N_6$ and Fe-$N_4$ Costructures Boost Oxygen Reduction Reaction in Both Alkaline and Acidic Media. *Adv. Mater.* **2021**, *33*, No. e2104718.
(58) He, Y.; Yang, X.; Li, Y.; Liu, L.; Guo, S.; Shu, C.; Liu, F.; Liu, Y.; Tan, Q.; Wu, G. Atomically Dispersed Fe-Co Dual Metal Sites as Bifunctional Oxygen Electrocatalysts for Rechargeable and Flexible Zn-Air Batteries. *ACS Catal.* **2022**, *12*, 1216−1227.
(59) Ravel, B.; Newville, M. ATHENA, ARTEMIS, HEPHAESTUS: data analysis for X-ray absorption spectroscopy using IFEFFIT. *J. Synchrotron Radiat.* **2005**, *12*, 537−541.
(60) Li, J.; Jiao, L.; Wegener, E.; Richard, L. L.; Liu, E.; Zitolo, A.; Sougrati, M. T.; Mukerjee, S.; Zhao, Z.; Huang, Y.; Yang, F.; Zhong, S.; Xu, H.; Kropf, A. J.; Jaouen, F.; Myers, D. J.; Jia, Q. Evolution Pathway from Iron Compounds to $Fe_1$(II)-$N_4$ Sites through Gas-Phase Iron during Pyrolysis. *J. Am. Chem. Soc.* **2020**, *142*, 1417−1423.
(61) Mehmood, A.; Pampel, J.; Ali, G.; Ha, H. Y.; Ruiz-Zepeda, F.; Fellinger, T. P. Facile Metal Coordination of Active Site Imprinted Nitrogen Doped Carbons for the Conservative Preparation of Non-Noble Metal Oxygen Reduction Electrocatalysts. *Adv. Energy Mater.* **2017**, *8*, 1701771.


https://doi.org/10.1021/acsomega.3c06005
*ACS Omega* 2023, 8, 41708−41717